Nonuniform Deployment of Autonomous Agents in Harbor-Like Environments

Suruz Miah[a] , Bao Nguyen[a] , Alex Bourque[a] , Davide Spinello[b]

[a] *Defence Research and Development Canada Center for Operational Research and Analysis, 101 Colonel By Drive Ottawa, Ontario, K1A 0K2, Canada,*
E-mail: {Suruz.Miah, Bao.Nguyen, Alex.Bourque}@drdc-rddc.gc.ca.

[b] *Department of Mechanical Engineering, University of Ottawa, Ottawa, Ontario, K1N 6N5, Canada,*
E-mail: Davide.Spinello@uottawa.ca.

We propose a nonuniform deployment strategy of a group of homogeneous autonomous agents in harbor-like environments. High value units berthed in the area need to be secured against external attacks. Defenders deployed in the area are expected to monitor, intercept, engage, and neutralize threats. In the framework of decentralized coordinated multi-agent systems, we model and simulate the optimal deployment of a group of mobile autonomous agents that accounts for a risk map of the area and the optimal trajectories that minimize the energy consumed to intercept a threat in a given area of interest. Theoretical results are numerically illustrated through simulations in a realistic harbor protection scenario.

Keywords: nonuniform deployment; threat interception; harbor protection.

1. Introduction

Cooperative missions with mobile sensor networks are being studied extensively from algorithmic to implementation aspects. Mobility, coupled with estimation, data fusion, and motion control algorithms, enables groups of mobile agents to coordinate in real-time to achieve specific objectives. These ideas have been applied to a variety of domains, including threat tracking [1–13], formation and coverage control [6, 14–25], rendezvous and deployment [26], environmental tracking and monitoring [27–30], and resource allocation problems with heterogeneous entities [31]. Comprehensive reviews can be found in [32–34], and several technical aspects are discussed in the book [35]. Here, we extend some of these ideas to securing harbors and ports against underwater threats, which is a problem with many opened challenges [36]. Securing ports against threats is especially acute when they are located near strategic choke points, such as the Strait of Hormuz, the Strait of Gibraltar, the Suez Canal, and the Panama Canal [36]. Among the most significant challenges in harbor protection study is that the visibility of both the attackers and agents is likely to be poor during their mission. In many realistic scenarios, sensory measurements are noisy and communication in the underwater domain is intermittent, leading to modeling frameworks similar to the one presented in [37] to study synchronization of intermittently coupled continuous-time nonlinear oscillators, with mean square convergence rates obtained in a discrete-time setting in [38, 39], and several extensions that include stochastic consensus protocols addressed in [40–42], and random link failures [43,44]. Here, in order to focus on the optimal deployment and interception with non-uniform risk, we assume that full communication exists among agents at all times, leaving the treatment of underlying time-varying communication networks to current and future work. This work contributes to the development of optimal strategy to deploy mobile autonomous agents and intercept threats in a harbor–like environment assuming that agents coordinate in a decentralized fashion by sharing information between them, without the intervention of an external unit. The area of deployment is assumed to be small enough so that information sharing capabilities allow each agent to communicate with the others in the group. Specifically, the main contributions of this paper are a set of possible solutions to address the following questions:

i) How and where to deploy agents throughout the harbor so that the likelihood of defending against threats is maximized?
ii) Given the agent's safe stand-off distance, how to intercept a threat in pre-specified reaction time while minimizing agent's actuator energy?

Deployment strategies developed here are of general interest in the broad field of cooperative missions with mobile multi-agent systems. However, they are illustrated herein for a harbor defence system taking into consideration a realistic harbor geometry, so that the abstraction of the formulation is immediately translated into suitable scenarios that facilitate the understanding of the applicability of

the proposed methods and solutions. It is assumed that the threats are initially outside the harbor's outermost boundary and the agents are placed closed to sensitive areas to be protected. The defence system is structured in two stages, where the first stage consists of deploying multiple mobile agents based on the risk distribution of the harbor. The risk zones inside the harbor are assumed to be known a priori, and they are encoded by a risk distribution with eventual non-uniformities. The area is then spatially partitioned according to Voronoi partitioning technique such that each Voronoi cell is assigned to a single agent. Like that, agents move in a fully decentralized fashion in the sense that each agent receives the position information from all other agents while employing its actions independently. Given the maximum sensor range, we determine the minimum number agents that needs to be deployed throughout the harbor. In the second stage, each agent will intercept the threats inside its own Voronoi cell taking into consideration its safe stand-off distance.

Yip et al. in [45] focused on formulating a stochastic model of the effectiveness of a harbor defence system against underwater threats. Their model is based on the assumption that only one agent is deployed against a single threat inside the harbor. In addition, the interception technique described in [45] assumes that the threat's trajectory is simply a straight line, which may be a too restrictive or non realistic hypothesis to model relevant real scenarios. Several research works have been conducted to protect harbors (civilian and military) and ports against underwater threats, see [46–51], for example, and some references therein. Authors in [52] presented a system of organic sensors coupled with one or more agents to protect high-value assets, where fuzzy logic algorithms were developed to determine priorities of both underwater and surface threats to be neutralized. However, a central control unit is required for their scenario to operate in real-time. Nevertheless, the nonuniform deployment of agents based on harbor's risk level are not considered in the literature to date. It turns out that the optimal deployment of agents and intercepting threats with minimum actuating energy are still among the main challenges, which we address in this paper. It is important to point out the fact that the proposed deployment strategy in a harbor defence system can be applied to scenarios where multiple defenders need to neutralize multiple threats. The work described herein exploits the concepts of multi-agent systems [53], the optimal discrete-time control and estimation theory [54].

The rest of the paper is outlined as follows. Section 2 gives the problem description and assumptions made throughout the paper including a high-level architecture of a harbor protection scenario. Section 3 details how to optimally deploy a set of homogeneous agents inside the harbor's inner reaction zone while maximizing coverage metric taking into account the risk maps. Section 4 describes how the agents optimally intercept a threat while minimizing their actuating energy. Section 5 presents the main theoretical results through computer simulations that encode the modelling assumptions. Section 6 gives the summary, conclusions, and potential future research avenues.

2. Assumptions, Harbor Architecture, and Modeling

Throughout this paper, scalar quantities will be denoted by lower-case letters, while vectors will be denoted by lower-case bold letters. Upper-case bold letters will denote matrices. For any positive integer n, $\mathbb{R}^n$ denotes the Euclidean space.

2.1. *Assumptions*

The current work relies on the following preliminary assumptions:

- Agents and threats operate in a 2D submerged workspace in the harbor.
- Agents can perfectly (without noise) communicate among them and each agent is responsible to intercept threats in its own zone of the harbor.
- Agents can estimate their position and velocity without noise.
- The harbor infrastructure is stationary.

The terms agent, interceptor, and defender will be used interchangeably throughout this paper.

2.2. *Harbor System Architecture*

A high-level architecture of a harbor defence system is depicted in Fig. 1. The shaded with zigzag pattern is the high value unit, that is located at the left of the harbor area. The presence of the high value unit introduces non-uniformity in the risk zone, and therefore it allows us to treat this important case. Sensors (sonars, for example) are mounted on the outermost trip-wire boundary. The purpose of the trip-wire sensors is to detect and track attackers while they are in the detect and track zones (see Fig. 1). In the scenario illustrated in Fig. 1, four agents are deployed inside the harbor area (inner reaction zone). As can be seen, the threats may enter from several directions (underwater or sideways, for instance) around the harbor. As such, the risk probability (which depends on the frequency of attacks by the threats) is also nonuniform. We consider a decentralized architecture in which there is no central control unit, as opposed to the scenario presented in [52]. Agents' optimal configurations in the inner reaction zone maximize a nonuniform coverage metric. In the presence of threats inside the inner reaction zone, each agent intercepts the threats that are inside its own Voronoi cell in the inner reaction zone of the harbor.

2.3. *Motion Models of Agents and Targets*

We consider a group of n homogeneous autonomous agents. Let γ and k denote the discrete sampling time interval and

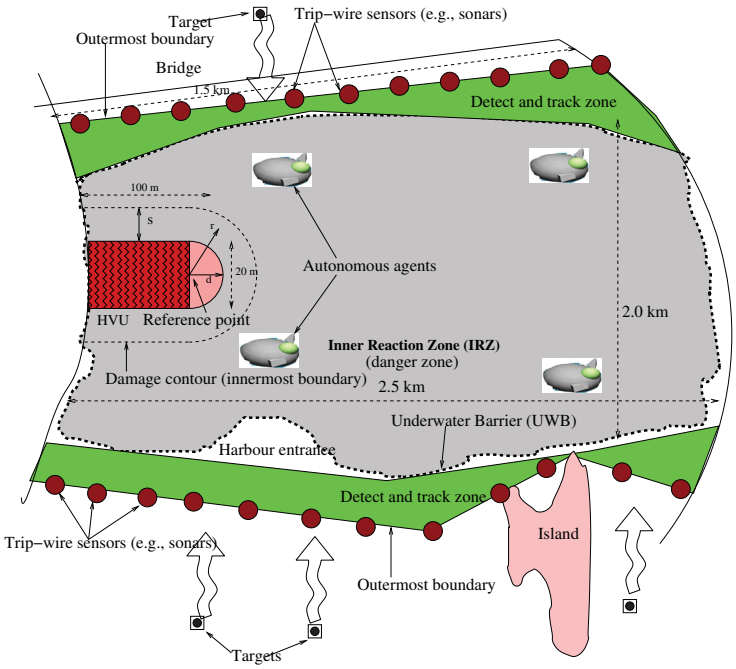

Fig. 1. Harbor protection system architecture.

discrete time index, respectively, characterizing the evolution of the agents in discrete time. The discrete time motion model of the ith, $i \in \{1, 2, \ldots, n\} \equiv \mathcal{I}$, agent is given by the following set of equations that describe the linearized kinematics of an accelerated material particle

$$\dot{\mathbf{p}}^{[i]} = \mathbf{u}^{[i]} \tag{1a}$$

$$\dot{\mathbf{v}}^{[i]} = \boldsymbol{\alpha}^{[i]}. \tag{1b}$$

where $\mathbf{p}^{[i]}(t) = \left[x^{[i]}(t),\ y^{[i]}(t)\right]^T$ is the 2D position, $\mathbf{v}^{[i]} = \left[v_x^{[i]}(t),\ v_y^{[i]}(t)\right]^T$ is the velocity at time $t \geq 0$, and $\mathbf{u}^{[i]}$ and $\alpha^{[i]}$ are the vectors of velocity and acceleration inputs, respectively. The kinematic model (1) approximates the 2D trajectory of the ith agent when it is required for agents to converge to a desired position with velocity determined by (1b).Similar to the agent model (1), we assume that each threat moves according to the linearized accelerated kinematics

$$\dot{\mathbf{s}} = \mathbf{u} \tag{2a}$$

$$\dot{\mathbf{v}} = \boldsymbol{\alpha} \tag{2b}$$

where $\mathbf{s}$ and $\mathbf{v}$ are the threat's 2D position and velocity vectors, respectively, with the corresponding 2D actuating inputs $\mathbf{u}$ and $\boldsymbol{\alpha}$.

3. Deployment of Agents

The agents are distributed in optimal locations inside the harbor, where the optimality is defined with respect to a generalized coverage metric that include the nonuniform risk map and the motion of the agents. The purpose of this section is to present motion coordination algorithms to optimally place agents. For that, we formally define the network model for the agents and the Voronoi tessellation of the inner reaction zone of the harbor.

3.1. *Harbor Partitioning and Network Model*

Let $\mathbf{p} = (\mathbf{p}^{[1]}, \ldots, \mathbf{p}^{[n]})$ be the collection of 2D positions of agents' network in the 2D inner reaction zone, $\mathcal{Q} \subset \mathbb{R}^2$, of the harbor. For optimal spatial placements and area coverage, agents partition the area to be covered using the generalized Voronoi partitioning technique [31, 55]. The Voronoi partition of the harbor is denoted by

$$\mathcal{V}(\mathbf{p}) = (\mathcal{V}_1(\mathbf{p}), \ldots, \mathcal{V}_n(\mathbf{p})),$$

where the ith Voronoi cell is defined by

$$\mathcal{V}_i(\mathbf{p}) = \{\mathbf{q} \in \mathcal{Q} \ :\ f(r_i) \geq f(r_j), \quad \forall j \in \mathcal{I} \setminus \{i\}\},$$

$\forall i \in \mathcal{I}$, $r_i = \|\mathbf{q} - \mathbf{p}^{[i]}\|$ is the Euclidean distance, and $f(\cdot)$ is the sensor performance function that will be defined in subsection 3.3. Therefore, the generators of the Voronoi partition are the states $(\mathbf{p}^{[1]}, \ldots, \mathbf{p}^{[n]})$. For simplicity, $\mathcal{V}_i(\mathbf{p})$ will be denoted by $\mathcal{V}_i$ throughout the paper. Intuitively, $\mathcal{V}_i$ represents an area where each point is better sensed by the ith agent than to all other agents. Interested readers are referred to [55] for the comprehensive study on Voronoi partitioning and its applications.

A network of agents in the inner reaction zone $\mathcal{Q} \subset \mathbb{R}^2$, is defined by the tuple $(\mathcal{I}, \mathcal{R}, \mathcal{E})$, where $\mathcal{R} \equiv$ set of agents $\equiv \{\mathcal{R}^i\}_{i\in\mathcal{I}} = \left\{\left(\mathcal{P}^{[i]}, \mathcal{U}^i, \mathcal{P}_0^{[i]}, \mathbf{f}^{[i]}\right)\right\}_{i\in\mathcal{I}}$, with $\mathcal{P}^{[i]} \subset \mathbb{R}^2$ is the state space of the ith agent, $\mathcal{U}^i$ is the set of control actions (accelerations) that define the trajectories, $\mathcal{P}_0^{[i]}$ is the set of initial states, and $\mathbf{f}^{[i]}$ is the physical state transition function of the ith agent. The communication edge map is given by $\mathcal{E} : \prod_{i=1}^n \mathcal{P}^{[i]} \mapsto \mathcal{I} \times \mathcal{I}$. The physical state and the initial physical state of the ith agent are $\mathbf{p}^{[i]} \in \mathcal{P}^{[i]}$ and $\mathbf{p}_0^{[i]} \in \mathcal{P}_0^{[i]}$, respectively. We refer to $\mathbf{p} = (\mathbf{p}^{[1]}, \ldots, \mathbf{p}^{[n]}) \in \prod_{i=1}^n \mathcal{P}^{[i]}$ as a state of the agents' network in the harbor's inner reaction zone.

Note that the map $\mathbf{p} \mapsto (\mathcal{I}, \mathcal{E}(\mathbf{p}))$ models the topology of the communication network among the agents. Hence, $(\mathcal{I}, \mathcal{E}(\mathbf{p}))$ denotes the communication graph. Two agents at locations $\mathbf{p}^{[i]}$ and $\mathbf{p}^{[j]}$ communicate if and only if the pair $(i, j) \in \mathcal{E}(\mathbf{p})$. The informal description of our deployment strategy for agents inside the harbor can be schematized as follows:

Step 0: Set up a communication protocol, such as agents will communicate with each other at discrete time instants during their entire mission. The ith agent performs *Step 1* and *Step 2* for each communication round:
Step 1: It broadcasts its own message (2D position and unique ID) to all other agents and receives the set of messages from all other agents.
Step 2: It updates its logical state (determining geometric centers, for example), which will be detailed later, of its own Voronoi region $\mathcal{V}_i$ inside the harbor.
Step 3: It updates its physical state $\mathbf{p}^{[i]}$ by moving towards the geometric center of $\mathcal{V}_i$ before the next communication round.

3.2. *Modeling Risk Zone*

Note that there might be different risk zones through which threats are likely to attack. Inspired by [56], we define risk zones in the harbor as the area where threats frequently enter to damage the high value unit. Following [17], we define the risk function $\phi : \mathcal{P} \longrightarrow \mathbb{R}_0^+$ as

$$\phi(\mathbf{q}) = e^{-\frac{1}{2}\left\{\frac{(q_x-\bar{q}_x)^2}{\sigma_x^2} + \frac{(q_y-\bar{q}_y)^2}{\sigma_y^2}\right\}}, \tag{3}$$

where $\mathbf{q} = [q_x, q_y]^T \in \mathcal{Q}$ is the position vector. Model (3) defines the risk zone centered around the location $(\bar{q}_x, \bar{q}_y)$ with standard deviations σ_x and σ_y along the X-axis and Y-axis, respectively. Note that the highest risk is at the location $(\bar{q}_x, \bar{q}_y)$. Since the risk function is nonuniform, this method leads to nonuniform distribution of agents, that are more densely deployed in areas with higher risk. The mass $M_\phi(\mathcal{V}_i)$ and the centroid $C_\phi(\mathcal{V}_i)$ of the Voronoi cell $\mathcal{V}_i$ are given by

$$M_\phi(\mathcal{V}_i) = \int_{\mathcal{V}_i} \phi(\mathbf{q}) d\Omega, \tag{4}$$

$$\mathbf{C}_\phi(\mathcal{V}_i) = \frac{1}{M_\phi(\mathcal{V}_i)} \int_{\mathcal{V}_i} \mathbf{q}\phi(\mathbf{q}) d\Omega, \tag{5}$$

respectively, with $d\Omega$ being the area element.

3.3. *Nonuniform Deployment*

Motivated by the locational optimization problem [55], we consider a generalized total coverage metric in terms of total power (signal strength) received by agents

$$H(\mathbf{p}, \mathcal{V}) = \sum_{i=1}^n \int_{\mathcal{V}_i} \phi(\mathbf{q}) f(r_i) d\Omega \tag{6}$$

where $r_i = \|\mathbf{q} - \mathbf{p}^{[i]}\|$, $\forall \mathbf{q} \in \mathcal{V}_i$. Note that $f(\cdot)$ is the agent's sensor performance defined by

$$f(r_i) = k \exp(-\beta r_i^2)$$

with $k > 0$ and $\beta > 0$. The metric (6) encodes how rich the coverage provided by the agents' network in $\mathcal{Q}$ is. In other words, higher H implies that the corresponding set of agents achieves better coverage of the area $\mathcal{Q}$. Commonly the Voronoi tessellation problem with mobile generators is formulated by modeling the dynamics of the agents as simple integrators, and therefore the coverage metric can be extremized by the well–known Lloyd algorithm [57]. Here, by considering accelerated particles taking into account the acceleration inputs, we want to maximize the coverage metric H as defined in (6), while the speeds of agents governed by (1b) reach zero at the optimal configurations of agents that eventually maximize the coverage. Note, however, that agents may reach optimal configurations before the acceleration inputs and velocity of the ith agent decay to zero as $t \to \infty$. An appropriate feedback law, defined in equation (11), for each of the input vectors in (1) dictates that each agent moves towards its generalized centroid with speed greater than the speed generated by the acceleration inputs. This guarantees that the system dynamics does not violate basic physics principles encoded by Newton's second law.

Using the results presented in [31, 53], the derivative of H_i in (6) with respect of $\mathbf{p}^{[i]}$ yields

$$\frac{\partial H^{[i]}}{\partial \mathbf{p}^{[i]}} = M_{\tilde{\phi}}(\mathcal{V}_i) \left(\mathbf{C}_{\tilde{\phi}}(\mathcal{V}_i) - \mathbf{p}^{[i]}\right), \tag{7}$$

where $\tilde{\phi}(\mathbf{q}, \mathbf{p}^{[i]}) = -2\phi(\mathbf{q}) \left(\partial f(r_i)/\partial(r_i^2)\right)$,

$$M_{\tilde{\phi}}(\mathcal{V}_i) = \int_{\mathcal{V}_i} \tilde{\phi}(\mathbf{q}, \mathbf{p}^{[i]}) d\Omega, \tag{8}$$

$$C_{\tilde{\phi}}(\mathcal{V}_i) = \frac{1}{M_{\tilde{\phi}}(\mathcal{V}_i)} \int_{\mathcal{V}_i} \mathbf{q}\tilde{\phi}(\mathbf{q}, \mathbf{p}^{[i]}) d\Omega. \tag{9}$$

It is worth pointing out that $\tilde{\phi}(\mathbf{q}, \mathbf{p}^{[i]})$ can be interpreted as modified risk levels that includes the agents' sensor performance in the harbor region $\mathcal{V}_i$, which is occupied by the ith agent and its corresponding mass and centroid are $M_{\tilde{\phi}}(\mathcal{V}_i)$ and $C_{\tilde{\phi}}(\mathcal{V}_i)$, respectively. From the above definition it follows that $\tilde{\phi} > 0$ since f is strictly decreasing in its argument.

The standard Lloyd descent algorithm [58] states that a necessary and sufficient condition for the agents to be in the optimal configuration that maximizes the coverage metric (6) (with constant density ϕ) is to asymptotically converge to the centroids of the Voronoi tessellation, *i.e.*, $\mathcal{P} = \{\mathbf{p}^{[i]}(t) | \mathbf{p}^{[i]}(t) = \mathbf{C}_{\phi}(\mathcal{V}_i)(t)\}$ as $t \to \infty$. Hence, if the agents (with kinematics (1)) are asymptotically deployed to the corresponding centroids, $C_{\tilde{\phi}}(\mathcal{V}_i)$, of the Voronoi tessellation, then the coverage metric is maximized as it is clear from (7) and therefore the configuration is optimal. Feedback laws that map to optimal trajectories of the closed loop system associated to the dynamics (1) are given in the following proposition, by showing that these trajectories belong to the largest invariant set of a quadratic Lyapunov function.

Let κ and μ_2 be positive constants. Before defining the feedback laws for the agent dynamics (1), we introduce the following assumption which relates tracking errors with respect to Voronoi centroids to actuation speed, posing that the actuation speed $\|\mathbf{v}^{[i]}\|$ cannot vanish before the ith agent converges to the centroid of the corresponding Voronoi cell.

Assumption 3.1.

$$\|\mathbf{v}^{[i]}\| \geq \bar{\kappa} \|\mathbf{C}_{\tilde{\phi}} - \mathbf{p}^{[i]}\|, \tag{10}$$

for some $\bar{\kappa} > 0$.

With the following proposition we give a feedback law for asymptotic convergence towards the centroids, and therefore optimal coverage in the sense of (6).

Proposition 3.2. Consider a group of n agents with dynamics (1). Let the function H defined in (6).

(1) Suppose that Assumption 10 holds $\forall t \geq 0$, the trajectories of the closed–loop system generated by the feedback laws (assuming $\mathbf{C}_{\tilde{\phi}} \neq \mathbf{p}^{[i]}$)

$$\mathbf{u}^{[i]} = \|\mathbf{v}^{[i]}\| \frac{\mathbf{C}_{\tilde{\phi}} - \mathbf{p}^{[i]}}{\|\mathbf{C}_{\tilde{\phi}} - \mathbf{p}^{[i]}\|}. \tag{11a}$$

$$\boldsymbol{\alpha}^{[i]} = -\kappa \mathbf{v}^{[i]}, \quad \kappa > 0. \tag{11b}$$

asymptotically drive the agents to the generalized centroids (9) with zero velocity, that is

$$\lim_{t \to \infty} \mathbf{p}^{[i]}(t) = \mathbf{C}_{\tilde{\phi}}, \quad \lim_{t \to \infty} \mathbf{v}^{[i]} = \mathbf{0}.$$

(2) The trajectories of the closed loop system associated to the feedback law (11) are optimal with respect to the metric (6).

Proof. Let

$$J = \sum_{i=1}^{n} \left(\frac{1}{2} \mu_1 \|\mathbf{v}^{[i]}\|^2 + \frac{1}{2} \mu_2 \|\mathbf{C}_{\tilde{\phi}} - \mathbf{p}^{[i]}\|^2 \right) \tag{12}$$

be a candidate Lyapunov function (cost function). With the substitution of feedback laws (11) the time derivative of the J along the trajectories is given by

$$\dot{J} = \sum_{i=1}^{n} \left(-\mu_1 \kappa \|\mathbf{v}^{[i]}\|^2 - \mu_2 \|\mathbf{v}^{[i]}\| \|\mathbf{C}_{\tilde{\phi}} - \mathbf{p}^{[i]}\| \right) \tag{13}$$

which is negative definite for nonzero positive constants μ_1 and μ_2. By using 10 the following bound follows

$$\begin{aligned} \dot{J} &= \sum_{i=1}^{n} \left(-\mu_1 \kappa \|\mathbf{v}^{[i]}\|^2 - \mu_2 \|\mathbf{v}^{[i]}\| \|\mathbf{C}_{\tilde{\phi}} - \mathbf{p}^{[i]}\| \right) \\ &\leq \sum_{i=1}^{n} \left(-\mu_1 \kappa \|\mathbf{v}^{[i]}\|^2 - \mu_2 \bar{\kappa} \|\mathbf{C}_{\tilde{\phi}} - \mathbf{p}^{[i]}\|^2 \right) < 0 \end{aligned} \tag{14}$$

for $\mathbf{v}^{[i]} \neq \mathbf{0}$ and $\mathbf{p}^{[i]} \neq \mathbf{C}_{\tilde{\phi}}$. By the global LaSalle's principle it follows that the asymptotically all trajectories are attracted into the largest invariant set of $\dot{J} = 0$, which implies point (1) since the largest invariant set includes only $\mathbf{v}^{[i]} = \mathbf{0}$ and $\mathbf{p}^{[i]} = \mathbf{C}_{\tilde{\phi}}$.

The proof of point (2) is completed by using a classical Lloyd algorithm argument, according to which $\mathbf{p}^{[i]} - \mathbf{C}_{\tilde{\phi}} = \mathbf{0}$ is the largest invariant set of the coverage metric H that is maximized along the trajectories associated with the feedback law $\mathbf{u}^{[i]}$, since such trajectories are proportional to its gradient ascent directions (see equation (7)). □

Note that the chain of inequalities (14) without the additional condition (10) would imply $\dot{J} = 0$ simply for $\|\mathbf{v}^{[i]}\| = \mathbf{0}$; therefore at the equilibrium the agents would not be required to converge to centroids of the Voronoi cells. Therefore, by requiring through condition (10) that the actuation velocity does not vanish before convergence to Voronoi centroids we also guarantee that equilibrium conditions correspond to optimal coverage.

4. Intercepting Threats

If threats leak through the underwater barrier, it is the agents' responsibility to intercept and engage them before they reach the damage contour of the high value unit. For that, an agent has to perform the following two major steps before engaging:

- Estimating threat's position and velocities.
- Intercept threats.

We consider on board sensory apparatuses taking noisy measurements of threats' trajectories at discrete times. Between two measurement times the threats' dynamics are approximated by a linearized stochastic process arising from the finite difference of (2)

$$\mathbf{g}[k+1] = \boldsymbol{\Phi} \mathbf{g}[k] + \boldsymbol{\Gamma} \left(\boldsymbol{\alpha}[k] + \boldsymbol{\omega}[k] \right), \tag{15}$$

where

$$\mathbf{\Phi} = \begin{bmatrix} 1 & 0 & \gamma & 0 \\ 0 & 1 & 0 & \gamma \\ 0 & 0 & 1 & 0 \\ 0 & 0 & 0 & 1 \end{bmatrix}, \ \mathbf{\Gamma} = \begin{bmatrix} \gamma^2/2 & 0 \\ 0 & \gamma^2/2 \\ \gamma & 0 \\ 0 & \gamma \end{bmatrix},$$

and γ is the sampling time. The state $\mathbf{g}[k] = [x[k],\ y[k],\ v_x[k],\ v_y[k]]^T$ includes 2D position and velocity at time instant k; $\boldsymbol{\alpha}[k] = [\alpha_x[k],\ \alpha_y[k]]$ is the 2D acceleration input at time instant k, $\mathbb{R}^2 \ni \boldsymbol{\omega}[k] \sim \mathcal{N}(0, \mathbf{\Lambda})$ is the process noise (white, zero-mean Gaussian random sequence) with $\mathbf{\Lambda}$ being the noise covariance matrix. The expected values of the threat's initial state and its error covariance are given by

$$E(\mathbf{g}[0]) = \hat{\mathbf{g}}[0],$$
$$E\left[(\mathbf{g}[0] - \hat{\mathbf{g}}_0)\,(\mathbf{g}[0] - \hat{\mathbf{g}}_0)^T\right] = \mathbf{P}[0].$$

Since the ith interceptor measures the line-of-sight (LOS) distance between itself and the threat at time instant k, the measurement model can be written as

$$\bar{\mathbf{z}}^{[i]}[k+1] = \mathbf{h}\left(\mathbf{g}[k+1], \boldsymbol{\xi}\right) = \mathbf{d}^{[i]}[k+1] + \boldsymbol{\xi}[k+1], \quad (16)$$

where $\mathbf{d}^{[i]}[k] = [d_1^{[i]}[k], \ldots, d_N^{[i]}[k]]^T$ with $d_\iota^{[i]}[k]$ being the Euclidean distance (LOS) given by

$$d_\iota^{[i]}[k+1] = \sqrt{(x^{[i]}[k+1] - x_\iota[k+1])^2 + (y^{[i]}[k+1] - y_\iota[k+1])^2},$$

N is the number of LOS distance measurements, $\iota = 1, \ldots, N$, $(x_\iota[k], y_\iota[k])$ is the 2D position of the threat corresponding to the measured distance $d_\iota^{[i]}$, and $\mathbb{R}^N \ni \boldsymbol{\xi}[k] \sim \mathcal{N}(0, \mathbf{\Sigma})$ is the measurement noise vector with zero-mean and $\mathbf{\Sigma}$ measurement noise covariance matrix. Having multiple line–of–sight (LOS) distance measurements between the ith interceptor and a threat at time instant k, the state $\hat{\mathbf{g}}[k]$ of a threat can be estimated using the Extended Kalman Filter (EKF) algorithm [59], since measurements are nonlinear functions of the state. The EKF employs the following two main phases at each time step for the interceptor to estimate the threat's state:

(1) A priori estimate (prediction): the threat's new state at time step $k+1$ is predicted using:

$$\hat{\mathbf{g}}_-[k+1] = \mathbf{\Phi}\hat{\mathbf{g}}_+[k] + \mathbf{\Gamma}\boldsymbol{\alpha}[k],\ \hat{\mathbf{g}}_+[0] = \hat{\mathbf{g}}[0], \quad (17)$$

where the subscripts "$_-$" and "$_+$" denote the a priori and a posteriori estimates, respectively. The error covariance matrix associated with this prediction is computed by:

$$\mathbf{P}_-[k+1] = \mathbf{\Phi}\mathbf{P}_+[k]\mathbf{\Phi}^T + \mathbf{\Gamma}\mathbf{\Lambda}\mathbf{\Gamma}^T,$$
$$\mathbf{P}_+[0] = \mathbf{P}[0].$$

(2) A posteriori estimate (correction): the Kalman gain is computed by

$$\mathbf{K}[k+1] = \mathbf{P}_-[k+1]\bar{\mathbf{H}}^T[k+1] \left(\bar{\mathbf{H}}^T[k+1]\mathbf{P}_-[k+1]\bar{\mathbf{H}}^T[k+1] + \mathbf{\Sigma}[k+1]\right)^{-1},$$

where $\bar{\mathbf{H}}[k+1]$ is the Jacobian with respect to the state $\mathbf{g}$ of the non-linear measurement model $\mathbf{h}(\cdot)$ in (16). The threat's state estimate is updated with current measurements using

$$\hat{\mathbf{g}}_+[k+1] = \hat{\mathbf{g}}_-[k+1] + \mathbf{K}[k+1]\left(\bar{\mathbf{z}}^{[i]}[k+1] - \mathbf{h}(\hat{\mathbf{g}}_-[k+1], \mathbf{0})\right)$$

The error covariance associated with the a posteriori estimate is updated by

$$\mathbf{P}_+[k+1] = (\mathbf{I}_4 - \mathbf{K}[k+1]\mathbf{H}[k+1])\mathbf{P}_-[k+1].$$

where $\mathbf{I}_4$ is the four dimensional identity matrix.

We assume that interceptors can estimate their position and velocity without noise. Similar to the model (15), the dynamic model (1) for the ith agent can be approximated in discrete–time by the linearized finite difference kinematics

$$\boldsymbol{\ell}^{[i]}[k+1] = \mathbf{\Phi}\boldsymbol{\ell}^{[i]}[k] + \mathbf{\Gamma}\boldsymbol{\alpha}^{[i]}[k], \quad (18)$$

where the state $\boldsymbol{\ell}^{[i]} = \left[x^{[i]}[k],\ y^{[i]}[k],\ v_x^{[i]}[k],\ v_y^{[i]}[k]\right]^T$ represents the state vector of 2D position and velocity at time instant k, and $\boldsymbol{\alpha}^{[i]}[k] = [\alpha_x^{[i]}[k],\ \alpha_y^{[i]}[k]]$ being the 2D acceleration input at time instant k. Agents use the threat's estimated state $\hat{\mathbf{g}}_+[k]$ to intercept, and the evolution of the error is a tracking measure. By subtracting (17) from (18) we obtain the following propagated error in discrete time

$$\mathbf{e}_-^{[i]}[k+1] = \mathbf{\Phi}\mathbf{e}_+^{[i]}[k] + \gamma\tilde{\boldsymbol{\alpha}}^{[i]}[k], \quad (19)$$

where $\mathbf{e}_+^{[i]}[k] = \boldsymbol{\ell}^{[i]}[k] - \hat{\mathbf{g}}_+[k]$ that is computed through EKF's prediction and update steps at each time instant k and $\tilde{\boldsymbol{\alpha}}^{[i]}[k] = \boldsymbol{\alpha}^{[i]}[k] - \boldsymbol{\alpha}[k]$. Given the reaction time t_r, the problem is to determine the optimal acceleration history $(u_x^{[i]}[k], u_x^{[i]}[k])$ (inputs to the agent) such that the agent can intercept the threat while maintaining its safe stand-off distance, r_w, before the threat reaches the damage contour around the high value unit. The detail derivations for generating $(u_x^{[i]}[k], u_x^{[i]}[k])$ are adapted from [60, Ch. 3] and are given in the Appendix 1.

5. Numerical Results

In this section, we provide a set of computer simulations to demonstrate the capability of a team of mobile agents in maximizing the probability of detecting a certain event in a harbor environment when individuals trajectories are

generated by the feedback law (11); in this case the performance metric is the nonuniform coverage metric defined in (6) which can be interpreted as the probability of detecting an event in a given area. In addition, we show how an agent intercepts a mobile threat within its own region in pre-specified reaction time while minimizing its actuating energy; in this case the performance measure is the position error (generated from the discrete time error model (19)) between an agent and a mobile target, while maintaining a safe stand-off distance. All simulations (both agent deployment and intercepting threats) are performed in discrete time with a sampling time interval $\gamma = 0.05$ s.

5.1. *Deployment*

The optimal coverage of the agents' nonuniform deployment in the harbor is illustrated by simulating a 2D inner reaction zone of the harbor with its boundary vertices at $(0.02, 0.02)$, $(1.2, 0.2)$, $(2, 0)$, $(2.2, 1)$, $(2, 2.5)$, $(0.6, 2.7)$, $(0, 2)$, $(0.05, 1.6)$, and $(0, 1)$ km. The distribution of risk zones throughout the harbor is given by (3), where the highest risk is in the region centered around $(\bar{x}, \bar{y})$ with $\sigma_x = 0.6$ km and $\sigma_y = 0.4$ km. It implies that threats can enter most-likely through regions centered around $(\bar{x}, \bar{y}) = (1.5, 0.2)$, $(0.4, 0.15)$, $(1.2, 2.5)$ km. Initially, 15 ($n = 15$) agents (hollow arrows with unique IDs $i = 1, \ldots, 15$) are placed close to the high value unit located at the middle of the left side of the harbor. The heading direction of each agent is toward the centroid of its corresponding Voronoi partition as computed by (5). The colormap on the right of Fig. 2 shows corresponding value of the risk level in the harbor, where 0 (zero) and 1 (one) correspond to lowest and highest risk level, respectively.

The evolution of agents' network at time $t \in [0, 60]$ s is determined through models (1) and (11) for $i = 1, \ldots, n$, and $\kappa = 1$. Their corresponding total coverage is computed by the coverage metric given in (6). The optimal configuration of the agents in total readiness time 60 s is revealed in Fig. 2 with the maximum coverage by the agents. Fig. 3 shows the normalized total coverage. The agents yields the maximum coverage of the harbor, which corresponds to unity (see Fig. 3). As expected, agents speeds decreasing while they move towards their optimal configurations. This model naturally leads to nonuniform deployment as dictated by the risk function, with higher risk zones more densely populated than lower risk zones. Nine agents are densely placed close to the harbor entrance and six agents are deployed from across the harbor entrance since there is a high probability of entering threats from these locations of the harbor.

5.2. *Intercepting Threats*

Assume that the agents are in optimal configurations as shown in Fig. 2(b). Here we show how the agent 14, for instance, intercepts a threat using its optimal acceleration inputs $\boldsymbol{\alpha}^{[14]}$ that minimize the actuating energy modeled by the cost function (A.1) while maintaining its safe stand-off distance. Since the harbor area that we have chosen is in the range of kilometer, for the purpose of showing the trajectory in meters we magnify the Voronoi cell of agent 14. For the proof of concept, we assume that the agent 14 is initially placed in the optimal loiter position (60 m, 10 m) in the inner reaction zone of the harbor. An alert has been sent to all agents that a threat is heading from the position $(98, -8)$ m towards the high value unit with an initial velocity of 1.2 m·s^{-1} (≈ 2.3 kn). Since the threat will surely be entering through Voronoi cell of agent 14, the agent 14 moves according to the kinematic model (18), where its acceleration inputs are computed by (A.8). Figs. 4(a) and 4(b) show their initial positions and velocities, respectively. The agent is always pointed towards the threat. The initial position error is about 42 m as shown in Fig. 5. Since the agent has to intercept the threat before it reaches the high value unit, it drastically increased the speed to ≈ 2.7 m·s^{-1} ($\approx$ 5.2kn) in about 4 s as shown in Fig. 4(b). Once the agent's position is about 15 m (safe stand-off distance, r_w) away from the threat, it maintains the same speed as the threat. This is clear from Fig. 5.

One important observation that can be made from this simulation results is that if the threat's speed is about 4 kn and it is initially about 42 m away from the agent, then it can intercept the threat in about 10 s and start engaging with its available weapons, for instance.

6. Summary and Conclusion

In this paper, we focus on an optimal deployment of multiple autonomous agents with the purpose of protecting a high value unit against multiple attacks in a harbor-like environment. A nonuniform risk distribution function is assigned to the area to be protected and agents are optimally distributed throughout the harbor to maximize a generalized coverage metric that encodes the non uniform risk distribution and the performance of sensory devices in detecting events in the area where they are deployed. The coverage metric is maximized along the trajectories generated by a feedback law with kinematic actuating actions. Agents are deployed more (less) densely in higher (lower) risk zones using Voronoi tessellation. Once threats penetrate the underwater barrier, the mobile agents are notified to intercept them. If a threat reaches in one of the Voronoi cells, the corresponding agent estimates the threat's position and velocities and intercept it in pre-specified reaction time. This is performed using the extended Kalman filter and the optimal linear quadratic control technique, which minimizes the agent's actuator energy that need to be applied to intercept the threat in its Voronoi cell.

Even though the current work focused in deploying agents patrolling in a harbor protection environment, the theoretical results are applicable to a general class of coverage optimization problems, such as nonuniform distribution of food supply among a group of animals, collecting scientific data in an underwater environment, and optimal

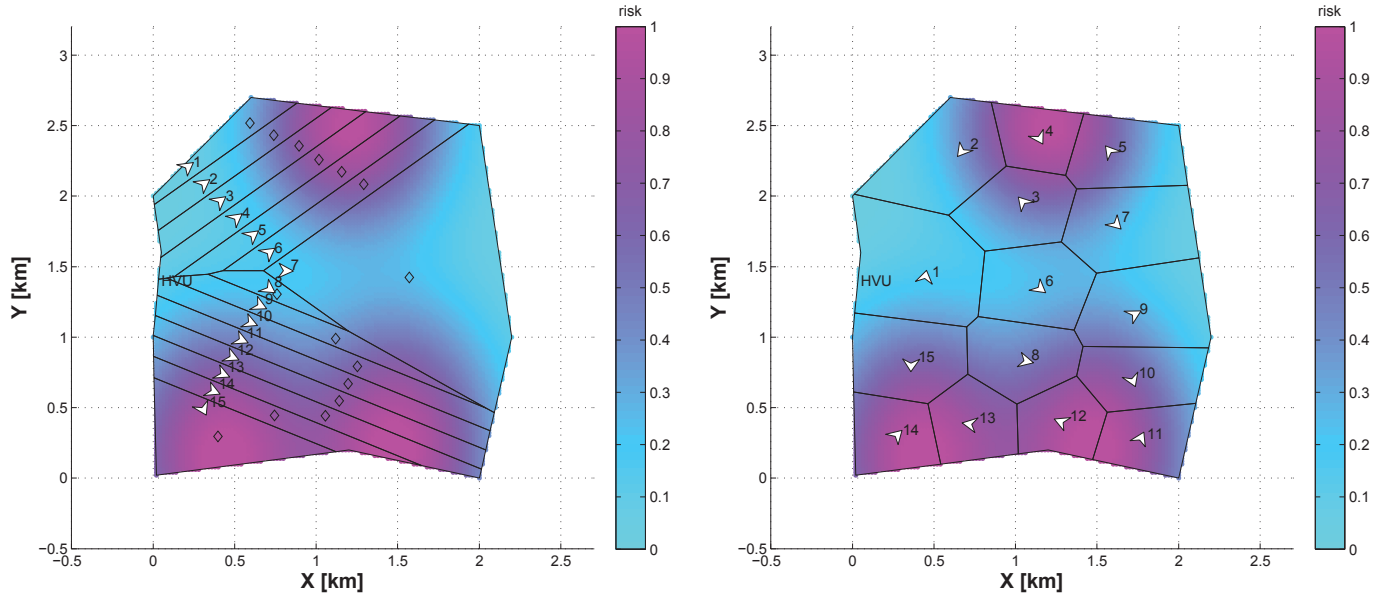

Fig. 2. Nonuniform coverage: agents' optimal configurations; colorbar represents risk level inside harbor

.

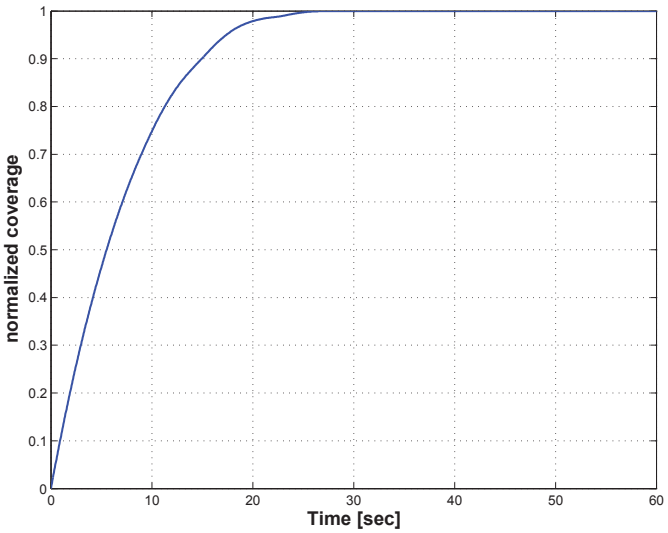

Fig. 3. Performance of the agents' nonuniform deployment.

configurations of a team of agents for estimating a target location.

The current harbor protection scenario assumes that agents are able to communicate among them perfectly (noise-free) without any information loss. However, this is not the case when a harbor contains islands or obstacles yielding intermittent communications among agents while accomplishing their missions. The optimal deployment of agents in the presence of such intermittent communications still remains a significant challenge and is a potential future research avenue, which is currently under investigation.

Acknowledgments

The authors would like to thank anonymous reviewers for their constructive feedback on this manuscript.

Appendix A Generating Optimal Acceleration Inputs for *i*th Agent

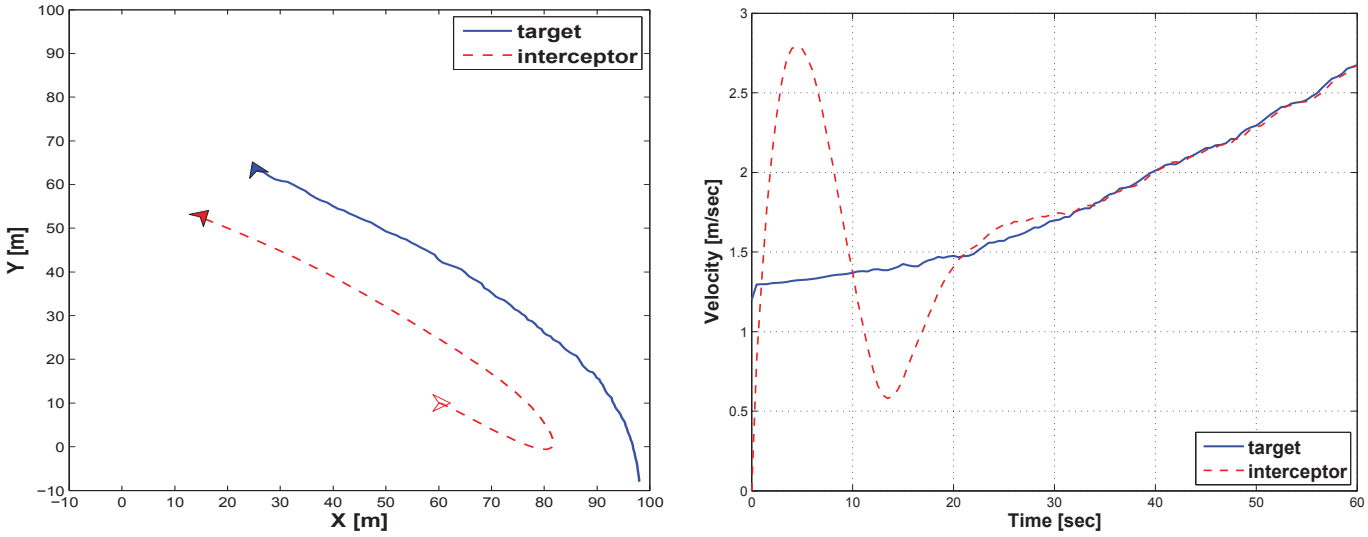

(a) (b)

Fig. 4. Intercepting a threat: (a) trajectories and (b) speed history; of the agent 14 and the threat.

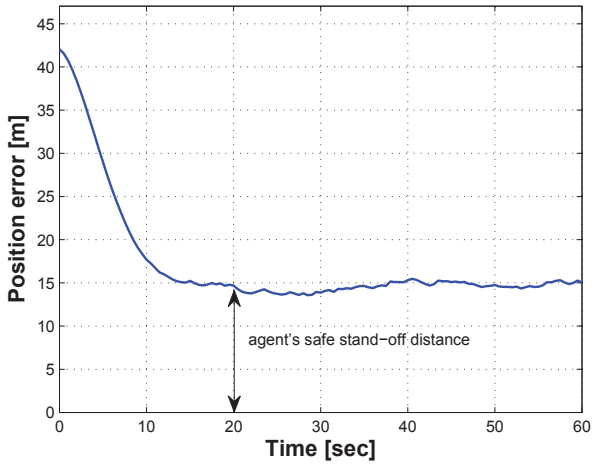

Fig. 5. Position error between the agent and the threat.

In this section, we will derive the optimal acceleration inputs $\boldsymbol{\alpha}^i[k]$, $k = 0, \ldots, k_f - 1$, for the ith,$i = 1, \ldots, n$, agent to intercept a threat within the reaction time t_r. We denote $t_k = \gamma k$ as the time at discrete index k and k_f corresponds to the reaction time t_r through $t_r = \gamma k_f$. For clarity, we simply drop the superscript $[i]$ and the subscript $+$ from the error vector $\mathbf{e}_+^{[i]}[k]$ and $\tilde{\boldsymbol{\alpha}} \equiv \tilde{\boldsymbol{\alpha}}^{[i]}$ in the rest of this section. We define ith agent's cost function as

$$J(\tilde{\boldsymbol{\alpha}}) = \frac{1}{2}\mathbf{e}^T(t_r)\mathbf{P}(t_r)\mathbf{e}^T(t_r) + \frac{1}{2}\sum_{k=0}^{k_f-1}\int_{t_k}^{t_{k+1}} \left(\mathbf{e}^T(t)\mathbf{Q}(t)\mathbf{e}(t) + \tilde{\boldsymbol{\alpha}}^T(t)\mathbf{R}(t)\tilde{\boldsymbol{\alpha}}(t)\right) \mathrm{d}t, \quad \text{(A.1)}$$

where $\mathbf{P}$, $\mathbf{Q} \in \mathbb{R}^4$ are positive (semi) definite symmetric matrices that represents the relative importance of position and velocity error components between the agent and the target. The matrix $\mathbf{R}$ is positive definite symmetric, which imposes restriction on the amount of energy required for acceleration inputs $\boldsymbol{\alpha}[k]$ (in terms of propeller thrust forces, for example). The objective at this stage is to minimize the cost $J(\tilde{\boldsymbol{\alpha}})$ for the ith agent. Since the agent can estimate the target's position and acceleration (as illustrated in section 4), the problem can be posed in terms of finding $\tilde{\boldsymbol{\alpha}}[k] \equiv \tilde{\boldsymbol{\alpha}}^{[i]}$ that solves the following optimization problem:

$$\inf_{\tilde{\boldsymbol{\alpha}}_k \in \mathbb{R}^2} J(\tilde{\boldsymbol{\alpha}}), \quad \text{(A.2)}$$

for $k = 0, \ldots, k_f - 1$.

The solution for $\tilde{\boldsymbol{\alpha}}[k]$ of the problem (A.2) follows the similar procedure illustrated in [60, Chapter 3]. We rewrite the error (19) as

$$\mathbf{e}(t) = \boldsymbol{\Phi}(t, t_k)\mathbf{e}[k] + \boldsymbol{\Gamma}(t)\tilde{\boldsymbol{\alpha}}[k], \tag{A.3}$$

for $t \in (t_k, t_{k+1}]$ and $\boldsymbol{\Phi}(t, t_k)$ is the possible time–varying state transition matrix. The cost functional (A.1) can be written as

$$J(\tilde{\boldsymbol{\alpha}}) = \frac{1}{2}\mathbf{e}^T(t_r)\mathbf{P}(t_r)\mathbf{e}(t_r) + \frac{1}{2}\sum_{k=0}^{k_f-1}\int_{t_k}^{t_{k+1}}\left(\begin{bmatrix}\mathbf{e}^T(t) & \tilde{\boldsymbol{\alpha}}^T(t)\end{bmatrix}\begin{bmatrix}\mathbf{Q}(t) & \mathbf{0}\\ \mathbf{0} & \mathbf{R}(t)\end{bmatrix}\begin{bmatrix}\mathbf{e}(t)\\ \tilde{\boldsymbol{\alpha}}(t)\end{bmatrix}\right)\mathrm{d}t. \tag{A.4}$$

By considering a discrete time implementation, for $t \in [t_k, t_{k+1}]$, $\tilde{\boldsymbol{\alpha}}[k]$ we approximate $\tilde{\boldsymbol{\alpha}}$ as constant, that is (*i.e.*, $\tilde{\boldsymbol{\alpha}}(t) = \tilde{\boldsymbol{\alpha}}[k]$, for $t \in [t_k, t_{k+1}]$). With this assumption and substituting $\mathbf{e}(t)$ from (A.3) in (A.4) yield

$$J(\tilde{\boldsymbol{\alpha}}) = \frac{1}{2}\mathbf{e}^T(t_r)\mathbf{P}(t_r)\mathbf{e}(t_r) + \frac{1}{2}\sum_{k=0}^{k_f-1}\int_{t_k}^{t_{k+1}}\Big(\begin{bmatrix}\mathbf{e}^T[k] & \tilde{\boldsymbol{\alpha}}^T[k]\end{bmatrix}\begin{bmatrix}\boldsymbol{\Phi}^T\mathbf{Q}\boldsymbol{\Phi} & \boldsymbol{\Phi}^T\mathbf{Q}\boldsymbol{\Gamma}\\ (\boldsymbol{\Phi}^T\mathbf{Q}\boldsymbol{\Gamma})^T & \mathbf{R} + \boldsymbol{\Gamma}^T\mathbf{Q}\boldsymbol{\Gamma}\end{bmatrix}\begin{bmatrix}\mathbf{e}[k]\\ \tilde{\boldsymbol{\alpha}}[k]\end{bmatrix}\Big)\mathrm{d}t, \tag{A.5}$$

with argument (t) dropped whenever no ambiguity arises. Defining

$$\begin{aligned}\hat{\mathbf{Q}}_k &= \int_{t_k}^{t_{k+1}}\boldsymbol{\Phi}^T(t, t_k)\mathbf{Q}(t)\boldsymbol{\Phi}(t, t_k)\mathrm{d}t,\\ \hat{\mathbf{M}}_k &= \int_{t_k}^{t_{k+1}}\boldsymbol{\Phi}^T(t, t_k)\mathbf{Q}(t)\boldsymbol{\Gamma}(t)\mathrm{d}t,\\ \hat{\mathbf{R}}_k &= \int_{t_k}^{t_{k+1}}\Big(\mathbf{R}(t) + \boldsymbol{\Gamma}^T(t)\mathbf{Q}(t)\boldsymbol{\Gamma}(t)\Big)\mathrm{d}t,\end{aligned} \tag{A.6}$$

the quadratic cost-functional (A.5) can be written as

$$J(\tilde{\boldsymbol{\alpha}}) = \frac{1}{2}\mathbf{e}_f^T\mathbf{P}_f\mathbf{e}_f + \frac{1}{2}\sum_{k=0}^{k_f-1}\begin{bmatrix}\mathbf{e}_k^T & \tilde{\boldsymbol{\alpha}}_k^T\end{bmatrix}\begin{bmatrix}\hat{\mathbf{Q}}_k & \hat{\mathbf{M}}_k\\ \hat{\mathbf{M}}_k^T & \hat{\mathbf{R}}_k\end{bmatrix}\begin{bmatrix}\mathbf{e}_k\\ \tilde{\boldsymbol{\alpha}}_k\end{bmatrix}\mathrm{d}t, \tag{A.7}$$

where we have adopted the compact notation $(\cdot)_f \equiv (\cdot)(t_r)$ and $(\cdot)_k \equiv (\cdot)[k]$. Given the agent's linear error model (19) and its quadratic cost functional given by (A.1), the agent's optimal acceleration error is given by the following linear-quadratic state feedback control law

$$\tilde{\boldsymbol{\alpha}}_k = -\mathbf{C}_k\mathbf{e}_k = -\Big(\hat{\mathbf{R}}_k + \boldsymbol{\Gamma}_k^T\mathbf{P}_{k+1}\boldsymbol{\Gamma}_k\Big)^{-1}\Big(\hat{\mathbf{M}}_k^T + \boldsymbol{\Gamma}_k^T\mathbf{P}_{k+1}\boldsymbol{\Phi}_k\Big)\mathbf{e}_k. \tag{A.8}$$

where $\mathbf{C}_k$ is the (2×4) optimal feedback gain matrix and $\mathbf{P}_k$ is the solution of the following discrete-time matrix Riccati equation

$$\mathbf{P}_k = \hat{\mathbf{Q}}_k + \boldsymbol{\Phi}_k^T\mathbf{P}_{k+1}\boldsymbol{\Phi}_k - \Big(\hat{\mathbf{M}}_k + \boldsymbol{\Phi}_k^T\mathbf{P}_{k+1}\boldsymbol{\Gamma}_k\Big)\Big(\hat{\mathbf{R}}_k + \boldsymbol{\Gamma}_k^T\mathbf{P}_{k+1}\boldsymbol{\Gamma}_k\Big)^{-1}\Big(\hat{\mathbf{M}}_k^T + \boldsymbol{\Gamma}_k^T\mathbf{P}_{k+1}\boldsymbol{\Phi}_k\Big) \tag{A.9}$$

with $\mathbf{P}_{k+1} = \mathbf{P}[k_f] \triangleq \mathbf{P}_f$.

For the agent to maintain a safe stand-off distance, the error vector $\mathbf{e}_k$, in (19) is replaced by $\mathbf{e}_k + [r_w\cos(\pi/4), r_w\cos(\pi/4), 0, 0]^T$, where r_w is the agent's safe stand-off distance. The derivation of (A.8) and (A.9) follow from [60, Chapter 3]. The following steps summarize the determination of the ith agent trajectory using optimal acceleration inputs $\boldsymbol{\alpha}^{[i]}[k]$:

Step 1: Define $\mathbf{Q}(t)$, $\mathbf{R}(t)$, and $\mathbf{P}(t_r)$ for the cost function (A.1).
Step 2: Compute $\hat{\mathbf{Q}}_k$, $\hat{\mathbf{M}}_k$, and $\hat{\mathbf{R}}_k$ using (A.6).
Step 3: Compute the matrix $\mathbf{P}_k$ backward using the discrete-time matrix Riccati equation (A.9).
Step 4: Compute $\tilde{\boldsymbol{\alpha}}_k \equiv \tilde{\boldsymbol{\alpha}}[k]$ using the control law (A.8).
Step 5: Compute the agent's optimal acceleration inputs by $\boldsymbol{\alpha}^{[i]}[k] = \tilde{\boldsymbol{\alpha}}[k] + \boldsymbol{\alpha}[k]$, where $\boldsymbol{\alpha}[k]$ is the targets acceleration input (assumed to be known).
Step 6: Generate agent's state (position and velocity) trajectory by (18).

References

[1] V. Sarma and S. Raju, Multisensor data fusion and decision support for airborne target identification, *IEEE Transactions on Systems Man and Cybernetics* **21** (SEP-OCT 1991) 1224–1230.

[2] M. E. Liggins II, C.-Y. Chong, I. Kadar, M. G. Alford, V. Vannicola and S. Thomopoulos, Distributed fusion architectures and algorithms for target tracking, *Preceedings of the IEEE* **85** (January 1997) 95–107.

[3] T. H. Chung, J. W. Burdick and R. M. Murray, Decentralized motion control of mobile sensing agents in a network, *Proceedings of the IEEE International Conference on Robotics and Automation*, Orlando, Florida (May 2006).

[4] T. H. Chung, V. Gupta, J. W. Burdick and R. M. Murray, On a decentralized active sensing strategy using mobile sensor platforms in a network, *Proceedings of the IEEE conference on Decision and Control*, Paradise Island, Bahamas (December 2004).

[5] S. Martínez and F. Bullo, Optimal sensor placement and motion coordination for target tracking, *Automatica* **42**(4) (2006) 661–668.

[6] P. Yang, R. A. Freeman and K. M. Lynch, Multi-Agent Coordination by Decentralized Estimation and Control, *IEEE Transactions on Automatic Control* **53** (Dec 2008) 2480–2496.

[7] Z. Tang and U. Ozguner, Cooperative sensor deployment for multi-target monitoring, *International Journal of Robust and Nonlinear Control* **18** (Jan 2008) 196–217.

[8] G. Shi and Y. Hong, Global target aggregation and state agreement of nonlinear multi-agent systems with switching topologies, *Automatica* **45** (May 2009) 1165–1175.

[9] Z. Wang and D. Gu, Cooperative Target Tracking Control of Multiple Robots, *IEEE Transactions on Industrial Electronics* **59** (Aug 2012) 3232–3240.

[10] C. Zhang and S. Fei, Energy efficient target tracking algorithm using cooperative sensors, *Journal of Systems Engineering and Electronics* **23** (Oct 2012) 640–648.

[11] H. S. Ramos, A. Boukerche, R. W. Pazzi, A. C. Frery and A. A. F. Loureiro, Cooperative target tracking in vehicular sensor networks, *IEEE Wireless Communications* **19** (Oct 2012) 66–73.

[12] Y.-C. Chen and C.-Y. Wen, Decentralized Cooperative TOA/AOA Target Tracking for Hierarchical Wireless Sensor Networks, *Sensors* **12** (Nov 2012) 15308–15337.

[13] L. Ma and N. Hovakimyan, Vision-Based Cyclic Pursuit for Cooperative Target Tracking, *Journal of Guidance Control and Dynamics* **36** (Mar-Apr 2013) 617–622.

[14] C. Belta and V. Kumar, Abstraction and control for groups of robots, *IEEE Transactions on Robotics* **20** (October 2004) 865–875.

[15] P. Ogren, E. Fiorelli and N. Leonard, Cooperative control of mobile sensor networks: Adaptive gradient climbing in a distributed environment, *IEEE Transactions on Automatic Control* **49** (Aug 2004) 1292–1302.

[16] J. Cortés, S. Martínez, T. Karatas and F. Bullo, Coverage control for mobile sensing networks, *IEEE Transactions on Robotics and Automation* **20**(2) (2004) 243–255.

[17] F. Lekien and N. E. Leonard, Nonuniform coverage and cartograms, *SIAM Journal on Control and Optimization* **48**(1) (2009) 351–372.

[18] J. A. Fax and R. M. Murray, Information flow and cooperative control of vehicle formations, *IEEE Transactions on Automatic Control* **49** (September 2004) 1465–1476.

[19] R. A. Freeman, P. Yang and K. M. Lynch, Distributed estimation and control of swarm formation statistics, *Proceedings of the American Control Conference*, Minneapolis, Minnesota USA (June 14-16 2006), pp. 749–755.

[20] K. Laventall and J. Cortés, Coverage control by multi-robot networks with limited-range anisotropic sensory, *International Journal of Control* **82**(6) (2009) 1113–1121.

[21] A. Jadbabaie, J. Lin and A. Morse, Coordination of groups of mobile autonomous agents using nearest neighbor rules, *IEEE Transactions on Automatic Control* **48** (Jun 2003) 988–1001.

[22] W. Ren and E. Atkins, Distributed multi-vehicle coordinated control via local information exchange, *International Journal of Robust and Nonlinear Control* **17** (Jul 2007) 1002–1033.

[23] Y. Cao and W. Ren, Multi-vehicle coordination for double-integrator dynamics under fixed undirected/directed interaction in a sampled-data setting, *International Journal of Robust and Nonlinear Control* **20** (Jun 2010) 987–1000.

[24] A. Kansal, W. Kaiser, G. Pottie, M. Srivastava and G. Sukhatme, Reconfiguration methods for mobile sensor networks, *ACM Transactions on Sensor Networks* **3** (Oct 2007).

[25] Y. Zou and P. R. Pagilla, Distributed Constraint Force Approach for Coordination of Multiple Mobile Robots, *Journal of Intelligent & Robotic Systems* **56** (Sep 2009) 5–21.

[26] R. Carli and F. Bullo, Quantized coordination algorithms for rendezvous and deployment, *SIAM Journal on Control and Optimization* **48**(3) (2009) 1251–1274.

[27] P. Ögren, E. Fiorelli and N. E. Leonard, Cooperative control of mobile sensor networks: Adaptive gradient climbing in a distributed environment, *IEEE Transactions on Automatic Control* **49**(8) (2004) 1292–1302.

[28] M. Porfiri, D. G. Roberson and D. J. Stilwell, Tracking and formation control of multiple autonomous agents: A two-level consensus approach, *Automatica* **43**(8) (2007) 1318–1328.

[29] S. Simic and S. Sastry, Distributed environmental monitoring using random sensor networks, *Proceeding of the 2nd International Workshop on Information Processing in Sensor Networks*, Palo Alto, CA (2003), pp. 582–592.

[30] S. Susca, F. Bullo and S. Martinez, Monitoring environmental boundaries with a robotic sensor network, *IEEE Transactions on Control Systems Technology* **16** (Mar 2008) 288–296.

[31] K. R. Guruprasad and D. Ghose, Heterogeneous locational optimization using a generalized voronoi partition, *International Journal of Control* **86** (April 2013) 977–993.

[32] I. F. Akyildiz, W. Su, Y. Sankarasubramaniam and E. Cayirci, Wireless sensor networks: a survey, *Computer Networks* **38** (2002) 393–422.

[33] J. Yick, B. Mukherjee and D. Ghosal, Wireless sensor network survey, *Computer Networks* **52**(12) (2008) 2292 – 2330.

[34] Y. Cao, W. Yu, W. Ren and G. Chen, An Overview of Recent Progress in the Study of Distributed Multi-Agent Coordination, *IEEE Transactions on Industrial Informatics* **9** (Feb 2013) 427–438.

[35] W. Ren and Y. Cao, *Distributed Coordination of Multi-agent Networks: Emergent Problems, Models, and Issues*Communications and Control Engineering, Communications and Control Engineering (Springer-Verlag, London, 2011).

[36] M. Vego, Harbour protection, *Naval Forces* **28**(3) (2007) 9–20.

[37] I. V. Belykh, V. N. Belykh and M. Hasler, Blinking

model & synchronization in small-world networks with a time-varying coupling, *Physica D* **195** (Aug 2004) 188–206.

[38] M. Porfiri, Stochastic synchronization in blinking networks of chaotic maps, *Phys. Rev. E* **85** (May 2012) p. 056114.

[39] M. Porfiri, A master stability function for stochastically coupled chaotic maps, *Europhys. Lett.* **96**(4) (2011) p. 40014.

[40] N. Abaid and M. Porfiri, Leader-follower consensus over numerosity-constrained random networks., *Automatica* **48**(8) (2012) 1845 – 1851.

[41] N. Abaid, I. Igel and M. Porfiri, On the consensus protocol of conspecific agents, *Linear Algebra Appl.* **437**(1) (2012) 221 – 235.

[42] N. Abaid and M. Porfiri, Consensus over numerosity-constrained random networks, *IEEE Trans. on Autom. Control* **56** (March 2011) 649–654.

[43] S. Kar and J. M. F. Moura, Distributed Consensus Algorithms in Sensor Networks With Imperfect Communication: Link Failures and Channel Noise, *IEEE Trans. on Signal Process.* **57** (Jan 2009) 355–369.

[44] S. Silva Pereira and A. Pages-Zamora, Mean Square Convergence of Consensus Algorithms in Random WSNs, *IEEE Trans. on Signal Process.* **58** (May 2010) 2866–2874.

[45] H. Yip, B. Nguyen, P. Grignan and Vermeij, Modeling and analysis for harbour protection against underwater terrorist attacks, Technical Report NURC-FR-2008-007, NATO Undersea Research Center (NURC) (2008).

[46] R. T. Kessel and R. D. Hollett, Underwater intruder detection sonar for harbour protection: State of the art review and implications, *IEEE International Conference on Technologies for Homeland Security and Safety*, (Ft. Belvoir Defense Technical Information Center OCT, Istanbul, Turkey, oct. 2006).

[47] A. Caiti, V. Morellato and A. Munafo, GIS-based performance prediction and evaluation of civilian harbour protection systems, *OCEANS – Europe*, Aberdeen (June 2007), pp. 1–6.

[48] R. T. Kessel, Protection in ports: countering underwater intruders, *UDT Europe, Undersea Defence Technology Europe*, Naples (5–7, June 2007).

[49] A. Burkle and B. Essendorfer, Maritime surveillance with integrated systems, *International Waterside Security Conference*, Carrara, Italy (November 2010), pp. 1–8.

[50] E. Simetti and M. Cresta, Towards the use of a team of USVs for civilian harbour protection: the problem of intercepting detected menaces, *OCEANS, IEEE - Sydney*, Sydney, NSW (May 2010), pp. 1–7.

[51] B. Nguyen and H. Yip, A stochastic model for layered defense: Ballistic missile defense and harbour protection, *International Waterside Security Conference*, Carrara, Italy (3–5 November 2010), pp. 1–8.

[52] C. Strode, D. Cecchi and V. Calabro, Simulation of a system of systems to protect high value assets from surface and underwater terrorist attack, *Undersea Defence Technology (UDT) Europe*, Cannes (June 2009).

[53] F. Bullo, J. Cortes and S. Martinez, *Distributed Control of Robotic Networks: A Mathematical Approach to Motion Coordination Algorithms* (Princeton University Press, Applied Mathematics Series, 2009).

[54] M. S. Miah, Design and implementation of control techniques for differential drive mobile robots: An rfid approach, PhD dissertation, School of Electrical Engineering and Computer Science, University of Ottawa (October 2012).

[55] A. Okabe, B. Boots, K. Sugihara and S. N. Chiu, *Spatial Tessellations: Concepts and Applications of Voronoi Diagrams*, second edn. (John Wiley & Sons, LTM, 2000).

[56] F. Lekien and N. E. Leonard, Nonuniform coverage and cartograms, *SIAM Journal of Control and Optimization* **48** (February 2009) 351–372.

[57] S. P. Lloyd, Least squares quantization in PCM, *IEEE Transactions on Information Theory* **28** (1982) 129–137.

[58] J. Cortes, S. Martinez, T. Kartas and F. Bullo, Coverage control for mobile sensing networks, *IEEE Transactions on Robotics and Automation* **20** (April 2004) 243–255.

[59] M. S. Miah and W. Gueaieb, A stochastic approach of mobile robot navigation using customized rfid systems, *International Conference on Signals, Circuits and Systems*, Jerba, Tunisia (November 2009).

[60] R. F. Stengel, *Optimal Control and Estimation* (Dover publications, inc., New York, 1994).